Antennas in Glass Interposer For sub-THz Applications

Kai-Qi Huang and Madhavan Swaminathan
3D Systems Packaging Research Center
School of Electrical and Computer Engineering
School of Materials Science and Engineering
Georgia Institute of Technology
Atlanta GA

***Abstract*—The development of next generation (6G) wireless communications is expanding new spectrum bands into sub-terahertz (sub-THz) frequencies above 100 GHz, and the antenna is a key component in RF front-end modules (FEM) for such frequency bands. This paper demonstrates integrated packaging solutions for antenna components in D-band by using glass-based package. With the assistance of full-wave simulation in HFSS software, we design sub-THz patch antennas operating at 140 GHz frequency band, and form arrays of such patch antennas for 5G+/6G (sub-THz) wireless communication applications. The patch antennas and feeding networks are implemented by microstrip structures on the top of the glass interposer, with ground planes beneath. Build-up layers of polymer dry films are laminated on a glass core substrate for multi-layer copper metallization, and copper structures are patterned on the polymer layers. For precise fabrication of the antenna and feeding structures in package, we utilise the semi-additive patterning process to deposit the copper structures. By forming patch antenna arrays, we obtain 10.6 dBi gain using a 4-element linear array and 16.2 dBi gain using a 4-by-4 2-D rectangular array. The feeding methods of patch arrays are also discussed in the paper. The bandwidths achieved for these arrays are 7% (10 GHz) and 5% (7 GHz), respectively, based on return loss measurements. The measurement results present good match to simulation models, considering the uncertainties at such high frequencies. We believe that this is the first demonstration of glass-based antenna-in-package solution in D-band frequencies. Antenna structures on glass substrates illustrated in this paper represent one of the basic building blocks for the heterogeneous integration of sub-THz FEM in glass-based packages.**

Keywords—antenna in package; sub-terahertz; glass packaging; 5G+/6G wireless communications; RF front-end module; semi-additive patterning

I. Introduction

As 5G technologies are undergoing deployment, research pioneers have started exploring wireless communication beyond 5G and furthermore for next generation (6G). One of the key technologies for 6G is to expand new spectrum bands into sub-terahertz (sub-THz) frequencies above 100 GHz [1]. At the current stage, the feasibility of RF systems in D-band (110 GHz – 170 GHz) are mostly investigated. To implement RF front-end modules (FEM) for such frequency bands, heterogeneous integration in glass-based packages is a good solution because of the advantages of glass-based packaging. In the sub-THz FEM, one of the key components is the antenna. The FEM configurations are highly dependent on the antenna properties. In-package planar antennas usually radiate either in broadside (perpendicular to the substrate surface) or end-fire (along the edge of the substrate) directions. Fig. 1(a) shows an FEM using broadside antennas on the top. Other components must fit beneath the antenna elements to achieve scalable arrays, so the transceiver chips are embedded in the substrate or mounted on the other side, and the heat will be removed from the back side. Fig 1(b) shows an FEM using end-fire antennas. This gives more space for chip assembly and thermal solution, but the FEM modules must be vertically mounted to a carrier board with narrow spacing to form 2-D arrays, and the RF loss will be higher because of longer interconnects. Thus, broadside antennas are preferred for large arrays. For 5G+/6G applications, antennas must support a reasonably wide bandwidth and support fairly high gain, with relatively simple structures of actual antennas to reduce the effect of process variations from fabrication. Considering the trade-off between performance and feasibility, microstrip patch antennas and arrays is an appropriate option [2]. The disadvantage of patch antennas is a relatively narrow bandwidth. However, at 140 GHz in D-band, a reasonable 10% of fractional bandwidth is 14 GHz of absolute bandwidth, which is almost equivalent to the entire 5G new radio bands from 24 – 39 GHz.

2377-5726/21/$31.00 ©2021 IEEE
DOI 10.1109/ECTC32696.2021.00188

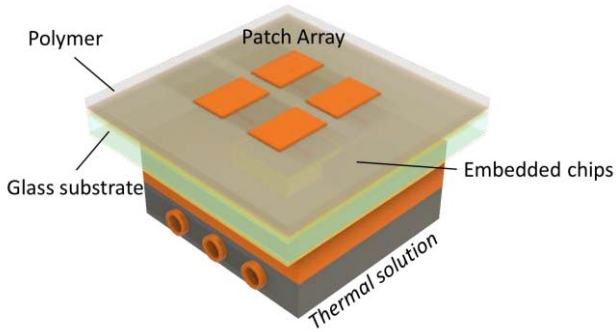

(a)

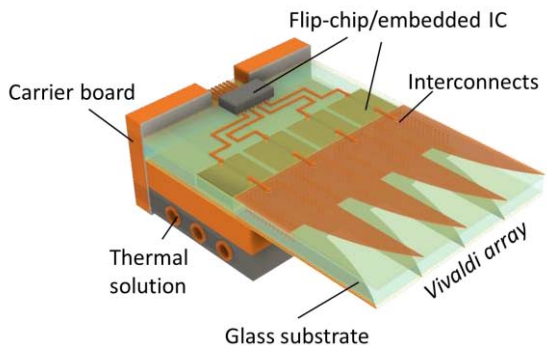

(b)

Fig. 1. RF front-end modules with (a) patch antennas (broadside radiation) and (b) Vivaldi antennas (end-fire radiation)

A few mm-wave/sub-THz antenna-in-package (AiP) manufacturing technologies have been previously reported, including low-temperature co-fired ceramics (LTCC) [3], polytetrafluoroethylene (PTFE) [4], and liquid crystal polymer (LCP) [5]. However, they either have limited performance or require comprehensive manufacturing processes [6]. In addition, surface roughness resulting from these processes can also degrade antenna performance. Glass interposer, with its smooth surfaces and good mechanical properties, provides the opportunity for implementing high-performance D-band AiP with low cost. In this paper, we demonstrate antenna structures on glass substrates, which represents a basic building block for integration in D-Band.

II. Design and Fabrication of Patch Antennas

A. Material Stack-up

Fig. 2 shows the material stack-up for the implementation of patch antennas. The core material is a 150mm × 150mm (6" × 6") AGC EN-A1 glass substrate with a thickness of 200µm. We laminate 15-µm dry-film polymer ABF GL102 onto both sides of the glass core, and plate copper inner layers as ground planes. Additional layers of 72.5-µm ABF GL102 polymer are then laminated and the copper structures on the outer layers are patterned using the semi-additive patterning process [7]. We select the polymer thickness of 72.5µm because a too thin substrate will limit the bandwidth and directivity of patch antennas, whereas an overly thick dielectric will support undesirable substrate modes and feedline radiation. The total height of the stack-up is less than 400µm. This double-sided stack-up balances the stress on both sides, thus avoids panel warpage during the fabrication process. ABF GL102 has dielectric constant (Dk) of 3.3 and dissipation factor (Df) of 0.0044. Although these data are specified at 5.8GHz, previous studies have shown the capability of such materials for sub-THz applications above 100 GHz as the properties are rather consistent [8]. To ensure the feasibility and quality of fabrication, the design rules include minimum line/space of 15 µm and via diameter of 72.5 µm (1:1 aspect ratio). This stack-up enables fine features on low-Dk, low-Df material, which benefits the performance of RF components at sub-THz frequencies.

B. Design of Patch Antennas and Arrays

We start the design by calculating the approximate dimensions (length L and width W) of a rectangular microstrip patch antenna on the glass stack-up operating at 140 GHz using the following equations [2]:

$$\mathrm{W} = \frac{c}{2f}\sqrt{\frac{2}{\epsilon_r+1}}, \tag{1}$$

and

$$\mathrm{L} = \frac{c}{2f\sqrt{\epsilon_{eff}}} - 2\Delta l, \tag{2}$$

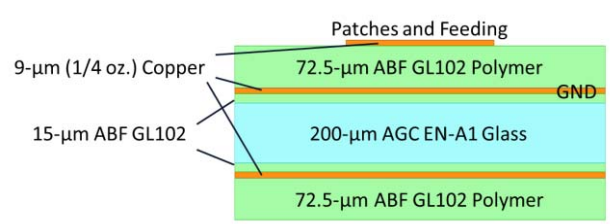

Fig. 2. Material stack-up for the implementation of patch antennas

where the effective permittivity

$$\epsilon_{eff} = \frac{\epsilon_r+1}{2} + \frac{\epsilon_r-1}{2} / \sqrt{1+\frac{12h}{W}}, \quad (3)$$

and the extension of length

$$\Delta l = 0.412\text{h}\frac{(\epsilon_{eff}+0.3)(W/h+0.264)}{(\epsilon_{eff}-0.258)(W/h+0.8)}. \quad (4)$$

The resonance of a patch antenna is mostly determined by its length, but weakly dependent on its width (which effects the effective permittivity and the extension of length). Generally, a wider patch supports larger bandwidth. However, the width should be less than twice the length to avoid higher-order resonant modes. A common practice is to set a 2:3 length-to-width ratio. By optimisation using full-wave simulation in ANSYS HFSS software starting with the length obtained from (1) – (4), we determine the length $L = 560\ \mu m$ and the width $W = 840\ \mu m$. The simulation estimates a gain of 6 dBi for an antenna element, radiating along the broadside direction, with a typical radiation pattern for patch antennas.

To obtain higher antenna gain, we form antenna arrays using multiple patch elements. Fig. 3(a) and 3(b) illustrates a 4-element linear array and a 4-by-4 rectangular array of patch antennas respectively. The antenna elements are placed half wavelength apart, which is

$$\text{P} = \lambda_0/2 = \frac{c}{2f} = \frac{3\times10^8\ m/s}{2\times140\ GHz} \cong 1.1\ mm, \quad (5)$$

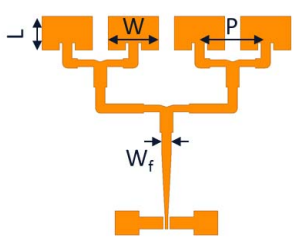

(a)

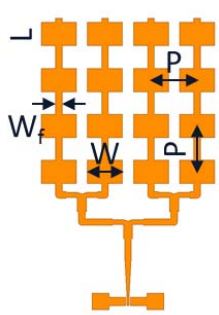

(b)

Fig. 3. Design of patch antenna arrays: (a) 4-element linear array; and (b) 4-by-4 2-D array

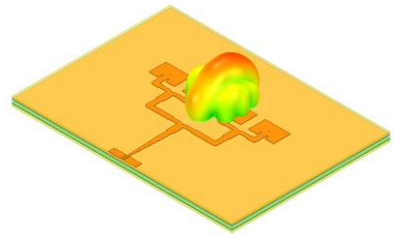

(a)

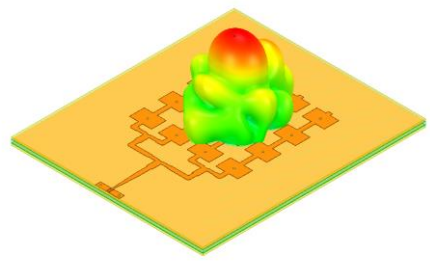

(b)

Fig. 4. Radiation patterns of (a) 4-element linear array and (b) 4-by-4 rectangular array

The feeding networks of the antenna arrays utilise microstrip lines on the same top layer. With a width of $W_f = 159\ \mu m$, the microstrip lines feeding into patches match to 50-Ω characteristic impedance. Antenna elements in an array can be fed in parallel or in series [9]. Parallel feeding provides better tunability and supports larger bandwidth. However, it requires power dividers to distribute the input power to each branch, which may not be feasibly for 2-D arrays using only the top layer for both patches and feedlines. Therefore, in our design, the linear array uses parallel feed, whereas the 4-by-4 array has a combination of parallel and series feeds. Simulation results of these structures show a gain of 10.6 dBi for the 4-element array and 16.2 dBi for the 4-by-4 array at 140 GHz, respectively. Both arrays radiate in the broadside direction, with Fig. 4 illustrating the radiation patterns.

C. Fabrication Processes

The primary fabrication processes that we utilise to construct copper structures on the glass-based stack-up include polymer lamination on glass and semi-additive patterning (SAP). Fig. 5 shows the multi-layer SAP process with schematic cross-section illustrations for each major step [8].

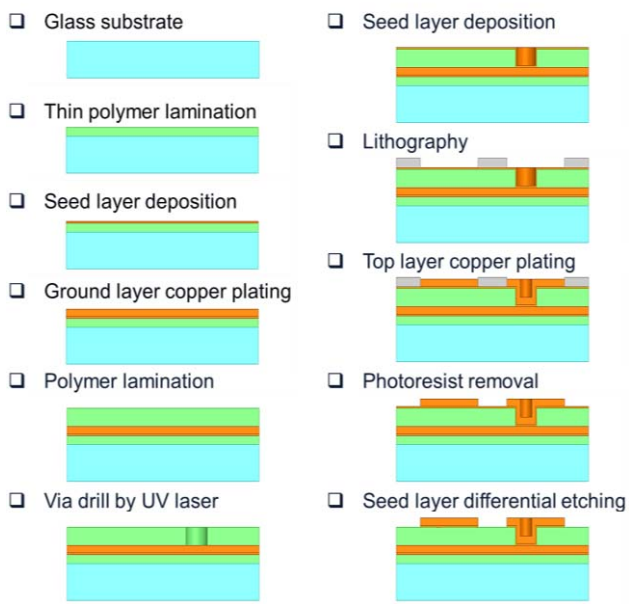

Fig. 5. Process flow of SAP fabrication of antenna on glass interposer (only one side is shown, not in scale)

The process starts with the lamination and curing of thin (typically 15µm) polymer dry films on a bare glass panel with silane treatment that coats the glass surface with silane vapour to improve adhesion between polymer and glass. We thereafter deposit a copper seed layer of a few hundred nanometres using a wet chemical deposition process, pattern the inner layer using lithography through dry-film negative photoresist, and grow the copper metallization within the opening of the developed photoresist by electroplating. Then the photoresist is stripped, and the seed layer is etched. The copper surface of inner layers is treated with Novabond wet process to improve adhesion, and the 72.5-µm polymer layers are laminated and cured. Subsequently, we apply an ultraviolet laser to drill blind vias that connect ground and top layers in the polymer film with optimised via ablation conditions. Similarly, another thin copper seed layer is deposited on the polymer, followed by patterning and electroplating of antennas structures on the outer copper layers. The desire patterns are obtained after stripping of the photoresist and differential etching of the excessive seed layer.

Compared to conventional etching process, SAP provides a rectangular cross-sectional profile of the deposited copper pattern through sidewall etching with minimal undercut. This advantage enables precise dimension control of fine copper structures for sub-THz applications.

III. Results and Analyses

The fabricated patch antenna array structures are shown in Fig. 6. To exam the fabricated samples, we measured the dimensions of these structures using an optical profiler. The results are listed in Table I. Note that copper patterns on the fabricated panel have shrunk by 4 – 5 µm from every edge of the structures compared to design, and this variation is consistent among structures over the panel. Reviewing the fabrication procedure, we suspect that over etching by an aggressive differential etcher is the primary cause, and insufficient dose time of lithography also contributed to the process variation. However, comparing the designed and fabricated dimensions, we notice that the fractional difference is not significant for patch antenna structures. The Feedlines are narrowed down for a few percent, but the

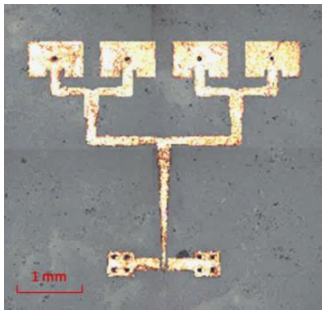

(a)

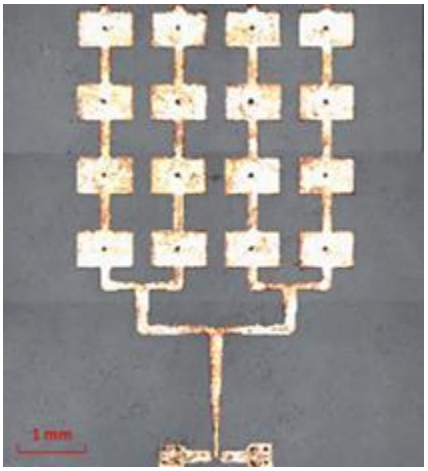

(b)

Fig. 6. Images of fabricated structures of (a) 4-element linear array and (b) 4-by-4 array of patch antennas and their feeding networks

TABLE I. COMPARISON OF DESIGNED AND FABRICATED DIMENSIONS

Dimensions	Designed	Fabricated	Difference
Patch length, L	560 µm	551 µm	-1.6%
Patch width, W	840 µm	831 µm	-1.1%
Element spacing, P	1.1 mm (λ/2)		
Feedline width, W_f	159 µm	150 µm	-5.7%
Probing pad width	50 µm	41 µm	-18%
Probing pad gap	30 µm	38 µm	+27%

impedance matching is quite tolerant to such variation. Thus, the patch antenna arrays will still operate appropriately. The most significant difference occurs at the ultra-fine co-planar structures of probing pad, resulting in considerable change in input impedance, but this can be corrected by re-normalizing the measurement S-parameters. Therefore, such process variations are acceptable for our design.

We measured return loss (S_{11}) of the samples using a vector network analyzer Agilent E8361C with a D-band frequency extender V06VNA2. A WR6 waveguide connects the frequency extender to a D-band ground-signal-ground probe 170-S-GSG-75-BT with 75-µm pitch. The equipment is configured for 1-port measurements in D-band. Fig. 7 (a) and (b) show the measurement results of the fabricated 4-element linear array and 4-by-4 2-D array respectively. Note that the probing pads have an impedance of 70 Ω by design, with tapered transitions to 50-Ω feedlines. The taper gives a gradual impedance slope to minimize reflection and mismatch. Although the fabricated pads are approximately 90 Ω, they still have a smooth transition to the 50 Ω feedline. Thus, the mismatch between the probe and pads is eliminated once we normalised the measured S_{11} parameters to 90 Ω input impedance. Based on the measurement results, the bandwidth of the 4-element linear array is 10 GHz or 7% with a resonance frequency at 137 GHz, compared to a 12-GHz bandwidth at 139 GHz by simulation; whereas the bandwidth for the 4-by-4 2-D array is 7 GHz or 5% with a resonance frequency at 142 GHz, compared to a 8-GHz bandwidth at 141 GHz by simulation. Comparing the plots of simulated and measured S_{11}, we notice that the measured results have a frequency shift of 2 – 3 GHz for both samples, or approximately 2% with respect to the 140-GHz operating frequency, which is mostly due to the process variations and measurement uncertainties. These results have shown fairly good correlation between measurement and simulation at such high frequencies. Table II compares the antenna parameters of AiP implementations in mm-wave/sub-THz frequencies using various technologies.

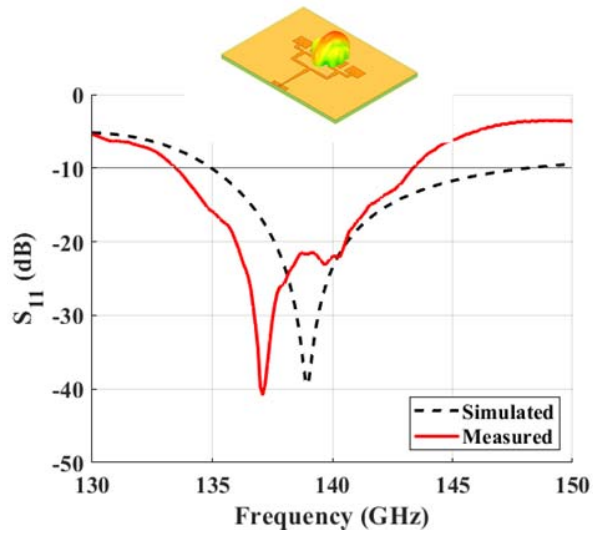

(a)

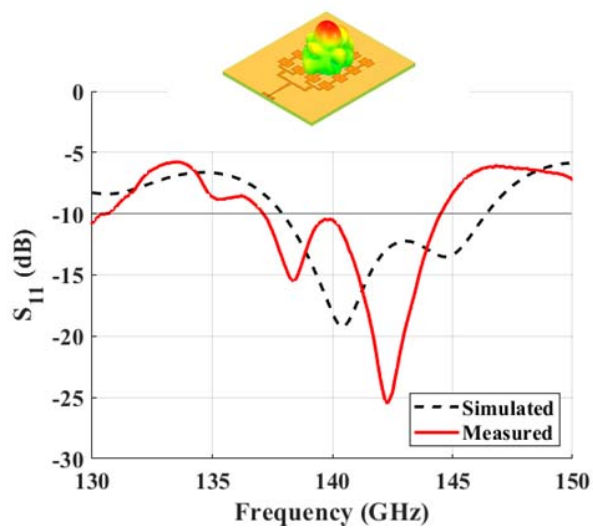

(b)

Fig. 7. Measured and simulated S_{11} results of (a) 4-element linear array and (b) 4-by-4 2-D array of patch antennas

We have demonstrated two examples of patch antenna arrays in this paper: a 4-element linear array with parallel feed that provides 10.6 dBi gain and a 4-by-4 2-D array with parallel/series feed that provides 16.2 dBi gain. In general, using similar array configurations and a combination of feeding methods, these antenna arrays are scalable. Hence, we can form arrays of certain element numbers to achieve antenna gain requirement for various applications in sub-THz frequencies.

TABLE II. COMPARISON OF MM-WAVE/SUB-THZ AIP PARAMETERS WITH VARIOUS IMPLEMENTATIONS

	Antenna type	Technology	Bandwidth (GHz)	Gain (dBi)	Size (mm × mm)
[3]	Grid array	LTCC	135 – 142	7.96	12 × 12
[4]	Pair-slot array	PTFE	76 – 77*	24.4	55 × 9.2
[5]	Grid array	LCP	136 – 157	14.5	10 × 10
This work	Patch array	Polymer build-up on glass	133 – 143	10.6	4.3 × 3
			137 – 144	16.2	4.3 × 6

* 15-dB return loss (otherwise 10 dB)

IV. CONCLUSIONS

This paper illustrates the feasibility of fabricating high-performance sub-THz AiP using glass interposer, which represents one of the basic building blocks for the heterogeneous integration of sub-THz FEM in glass-based packages. We have designed and fabricated patch antennas and antenna arrays for 5G+/6G sub-THz applications. The implementation of patch antennas is based on glass substrate with laminated polymer dry films, and the antenna structures are fabricated using SAP process, which ensures the precision of the structures and the performance of the components. Examples of a 4-element linear array with parallel feed and a 4-by-4 2-D array with combined parallel and series feeds are presented in particular. These antenna arrays, operating at around 140 GHz in D-band, have reasonable bandwidth and antenna gain. The fabricated antenna samples have shown good correlation for the return loss between measurement results and simulation models. These results have also indicated the scalability of such antenna arrays using certain number of elements for specific gain requirements of various applications. We believe that this is the first demonstration of glass-based AiP solution in D-band frequencies.

ACKNOWLEDGEMENT

This work was supported in part by ASCENT, one of six centers in JUMP, a Semiconductor Research Corporation (SRC) program sponsored by DARPA.

This work was also supported by Georgia Tech Packaging Research Center (GT–PRC) industry consortium for fabrication.

REFERENCES

[1] H. Viswanathan and P. E. Mogensen, "Communications in the 6G Era," in IEEE Access, vol. 8, pp. 57063-57074, 2020, doi: 10.1109/ACCESS.2020.2981745.

[2] Constantine A. Balanis, *Antenna Theory—Analysis and Design*, 3rd ed., Chapter 14, John Wiley & Sons, Inc., Hoboken, NJ, 2005, pp. 811-820.

[3] C. Kärnfelt, B. Zhang and H. Zirath, "A QFN packaged grid array antenna in low dielectric constant LTCC for D-band applications," 2016 IEEE MTT-S International Microwave Workshop Series on Advanced Materials and Processes for RF and THz Applications (IMWS-AMP), Chengdu, China, 2016, pp. 1-4, doi: 10.1109/IMWS-AMP.2016.7588410.

[4] T. Shijo, S. Obayashi and T. Morooka, "Design and development of 77-GHz pair-slot array antenna with single-mode post-wall waveguide for automotive radar," 2011 IEEE International Symposium on Antennas and Propagation (APSURSI), Spokane, WA, USA, 2011, pp. 476-479, doi: 10.1109/APS.2011.5996748.

[5] B. Zhang, C. Kärnfelt, H. Gulan, T. Zwick and H. Zirath, "A D - Band Packaged Antenna on Organic Substrate With High Fault Tolerance for Mass Production," in IEEE Transactions on Components, Packaging and Manufacturing Technology, vol. 6, no. 3, pp. 359-365, March 2016, doi: 10.1109/TCPMT.2016.2519522.

[6] A. Lamminen, J. Säily, J. Ala-Laurinaho, J. de Cos and V. Ermolov, "Patch Antenna and Antenna Array on Multilayer High-Frequency PCB for D-Band," in IEEE Open Journal of Antennas and Propagation, vol. 1, pp. 396-403, 2020, doi: 10.1109/OJAP.2020.3004533.

[7] P. M. Raj, C. Nair, H. Lu, F. Liu, V. Sundaram, D. W. Hess, and R. Tummala, "“zero-undercut” semi-additive copper patterning - a breakthrough for ultrafine-line RDL lithographic structures and precision RF thinfilm passives," 2015 IEEE 65th Electronic Components and Technology Conference (ECTC), San Diego, CA, USA, 2015, pp. 402-405, doi: 10.1109/ECTC.2015.7159624.

[8] Mutee ur Rehman, S. Ravichandran, S. Erdoğan and M. Swaminathan, "W-band and D-band Transmission Lines on Glass Based Substrates for Sub-THz Modules," 2020 IEEE 70th Electronic Components and Technology Conference (ECTC), Orlando, FL, USA, 2020, pp. 660-665, doi: 10.1109/ECTC32862.2020.00109.

[9] Thomas A. Milligan, Modern Antenna Design, 2nd ed., Chapter 6, John Wiley & Sons, Inc., Hoboken, NJ, 2005, pp. 327-330.